

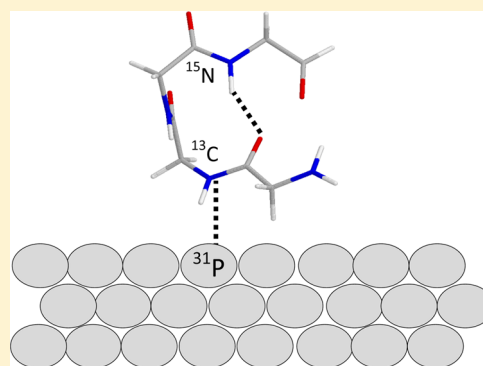
Phosphorylation and Ionic Strength Alter the LRAP–HAP Interface in the N-Terminus

Jun-xia Lu, Yimin Sharon Xu, and Wendy J. Shaw*

Pacific Northwest National Laboratory, Richland, Washington 99354, United States

S Supporting Information

ABSTRACT: The conditions present during enamel crystallite development change dramatically as a function of time, including the pH, protein concentration, surface type, and ionic strength. In this work, we investigate the role that two of these changing conditions, pH and ionic strength, have in modulating the interaction of the amelogenin, LRAP, with hydroxyapatite (HAP). Using solid-state NMR dipolar recoupling and chemical shift data, we investigate the structure, orientation, and dynamics of three regions in the N-terminus of the protein: L¹⁵ to V¹⁹, V¹⁹ to L²³, and K²⁴ to S²⁸. These regions are also near the only phosphorylated residue in the protein pS¹⁶; therefore, changes in the LRAP–HAP interaction as a function of phosphorylation (LRAP(–P) vs LRAP(+P)) were also investigated. All of the regions and conditions studied for the surface immobilized proteins showed restricted motion, with indications of slightly more mobility under all conditions for L¹⁵(+P) and K²⁴(–P). The structure and orientation of the LRAP–HAP interaction in the N-terminus of the phosphorylated protein is very stable to changing solution conditions. From REDOR dipolar recoupling data, the structure and orientation in the region L¹⁵V¹⁹(+P) did not change significantly as a function of pH or ionic strength. The structure and orientation of the region V¹⁹L²³(+P) were also stable to changes in pH, with the only significant change observed at high ionic strength, where the region becomes extended, suggesting this may be an important region in regulating mineral development. Chemical shift studies also suggest minimal changes in all three regions studied for both LRAP(–P) and LRAP(+P) as a function of pH or ionic strength, and also reveal that K²⁴ has multiple resolvable resonances, suggestive of two coexisting structures. Phosphorylation also alters the LRAP–HAP interface. All of the three residues investigated (L¹⁵, V¹⁹, and K²⁴) are closer to the surface in LRAP(+P), but only K²⁴S²⁸ changes structure as a result of phosphorylation, from a random coil to a largely helical structure, and V¹⁹L²³ becomes more extended at high ionic strength when phosphorylated. These observations suggest that ionic strength and dephosphorylation may provide switching mechanisms to trigger a change in the function of the N-terminus during enamel development.



Dental enamel is the hardest tissue in the human body, with a high mineral content and crystals which are elongated along the *c*-axis.¹ Amelogenins comprise more than 90% of protein in the developing enamel matrix and are thought to be a key constituent in shaping the resulting crystal, despite their predominantly hydrophobic composition. The eight acidic, five basic, and one phosphorylated amino acid residues that are present in full-length amelogenin are located almost entirely in the N- and C-terminal domains (Table 1).¹ Because of the charge localization, both domains are believed to be important for interaction with developing enamel crystals, and there is significant experimental evidence to support this hypothesis.^{2,3} Solid-state NMR (SSNMR) studies have demonstrated that both the N- and C-terminus of the naturally occurring amelogenin splice variant, leucine-rich amelogenin protein (LRAP), are close enough to the HAP surface to play a role in binding and crystal growth.^{4–7} *In vitro* studies show a reduction of the crystal–amelogenin interaction in the absence of the C-terminus, demonstrating its importance.^{8,9} Adsorption isotherms of peptides of the N- and C-termini of amelogenin, as well as the full length protein, show that the C-terminus does

not bind well to HAP without the rest of the protein, demonstrating that both the N- and C-terminal regions are important in the interaction of amelogenin with HAP.¹⁰

During normal enamel development, large changes in the environmental conditions are observed, including changes in solution pH (5.8 to 8.5),^{11–13} ionic strength (up to 0.165 M),^{11–14} crystal type (OCP and HAP),¹ and protein concentration (up to 200 mg/mL). These conditions have been observed to significantly affect the quaternary structure of amelogenin (nanospheres), resulting in changes in average size (5–100 nm) as well as the size distribution.^{15–18} Additionally, solution-state NMR studies have shown differences in secondary structure as a function of pH.^{19–22} Phosphorylation has also been shown to influence a conformational change in amelogenins, in solution, and on the surface,^{4,23} suggesting that phosphorylation may play a role in regulating protein–mineral

Received: January 18, 2013

Revised: March 11, 2013

Published: March 11, 2013



Table 1. Primary Structures of Mouse Amelogenin and LRAP^a

Amelogenin	MPLPPHPGSPGYINL pSyE VLTP L KWYQSM R Q P #PLSPIL P EL P LEAWPAT DKT KREE V D
LRAP-L ¹⁵ V ¹⁹ (-P)	MPLPPHPGSPGYIN L S Y E V LT P LKWYQSM R Q P PLSPILPELPLEAWPATDKTKREEVD
LRAP-L ¹⁵ V ¹⁹ (+P)	MPLPPHPGSPGYIN LpSyE VLTP L KWYQSM R Q P PLSPILPELPLEAWPATDKTKREEVD
LRAP-V ¹⁹ L ²³ (-P)	MPLPPHPGSPGYINLS Y E V LT P LKWYQSM R Q P PLSPILPELPLEAWPATDKTKREEVD
LRAP-V ¹⁹ L ²³ (+P)	MPLPPHPGSPGYINL pSyE VLT P LKWYQSM R Q P PLSPILPELPLEAWPATDKTKREEVD
LRAP-K ²⁴ S ²⁸ (-P)	MPLPPHPGSPGYINLSYEVLT P LKWYQ S M R Q P PLSPILPELPLEAWPATDKTKREEVD
LRAP-K ²⁴ S ²⁸ (+P)	MPLPPHPGSPGYINL pSyE VLTP L KWYQ S M R Q P PLSPILPELPLEAWPATDKTKREEVD
Central portion of amelogenin (#)	#YPSYGY E PMGGWLHHQHIVLSQQHPPSHTLQPHHHLVVPAQQPVAPQQPMMPVPGHHSMTPTQHHQPNIPPSAQPFQPFQQAIPPQSHQPMQPSPLHPMQPLAPQPPLPLFSMQ

^aThe charged residues are highlighted in red (acidic) and blue (basic) in the full length structure, showing the localization in the N- and C-termini. The hydrophobic central portion of amelogenin is indicated by “#” and is shown at the bottom of the table. The six isotopically labeled samples prepared for these studies are shown, with isotopic labels indicated by **bold** (¹³C′) and **bold-underlined** (¹⁵N), and phosphorylation indicated by a red pS at position 16.

interactions. The sensitivity of the quaternary structure of amelogenin to changing solution conditions and phosphorylation suggests that these conditions may also change the secondary structure and the interaction of amelogenins with HAP, where the protein is in its functional form. Understanding how each of these factors influences the amelogenin–HAP interaction is important in developing a mechanism for the organized growth which results in enamel crystals.

In our lab, we have demonstrated that solid-state NMR is a powerful technique to study the structure, orientation, and dynamics of biomineralization proteins bound to surfaces under biologically relevant conditions.^{4–7} We have used LRAP, shown in Table 1, which contains only the highly conserved N-terminus (first 33 residues) and C-terminus (last 26 residues) of amelogenin. With this truncated amelogenin, we have provided the first molecular level structural insight into an amelogenin–HAP interface. We have shown that the LRAP C-terminus is largely random coil when adsorbed to HAP and is very close to the HAP surface (¹³C′ is 5.7–7 Å from the HAP surface for the sites studied). Although the LRAP C-terminus interacts closely with HAP, it also exhibits a significant mobility, prompting our investigation of the N-terminal region. In the un-phosphorylated protein, the N-terminus has a more helical character than the C-terminus and the backbone is further from the surface of HAP (8–9 Å), but still close enough to interact. Upon phosphorylation of S¹⁶, a naturally occurring site of phosphorylation, regions near the pS¹⁶ residue moved closer to the surface of HAP (5.3–7.0 Å), with no accompanying structural changes in this region (L¹⁵ to L²³) due to phosphorylation.⁴ However, binding LRAP to HAP did result in an increase in the helical nature of LRAP in this region. In this work we extend the solid-state NMR studies of the N-terminal region of LRAP and investigate the role of the changing conditions during enamel growth. We investigate the effects of pH, ionic strength, and phosphorylation on the secondary structure, dynamics, and protein orientation, using both dipolar recoupling and chemical shift SSNMR measurements.

EXPERIMENTAL METHODS

Materials. Labeled amino acids were purchased from Cambridge Isotopes (Andover, MA). Fmoc-protected labeled amino acids were prepared as previously described⁷ using standard procedures.^{24,25} The HAP (90 m²/g) used for binding was made and characterized according to literature preparation²⁶ and stored as a slurry (28.9 mg/mL) to maintain the high surface area.

Protein Synthesis and Purification. Site-specifically labeled LRAP proteins were prepared by solid phase peptide synthesis using Fmoc chemistry by the Protein Chemistry Technology Center, University of Texas (Dallas, TX). Phosphorylated LRAP (LRAP(+P)) and non-phosphorylated LRAP (LRAP(-P)) were synthesized with an isotopically labeled backbone carbonyl carbon (¹³C′) and amide nitrogen (¹⁵N) introduced in the *i* and *i* + 4 positions, respectively (Table 1). Three labeling schemes were incorporated, resulting in six protein samples: L¹⁵V¹⁹(-P), L¹⁵V¹⁹(+P), V¹⁹L²³(-P), V¹⁹L²³(+P), K²⁴S²⁸(-P), and K²⁴S²⁸(+P). Each sample was purified by reverse phase HPLC using buffer A, 0.1% trifluoroacetic acid in water; buffer B, 0.1% trifluoroacetic acid in acetonitrile. LRAP eluted at 54% B. Mass spectroscopy was used to characterize the purity and molecular weight of the proteins. After purification, proteins were lyophilized for storage until ready for use.

Protein Solutions. For each labeled protein sample, the protein was bound to HAP under five different solution conditions (Table 2). The “standard condition” is defined as pH = 7.4 and IS = 0.15, and the solution was prepared as follows. A buffer saturated with respect to HAP (SCP) was

Table 2. The Five Sample Conditions Used To Study LRAP Bound to HAP (Marked with an X)

IS (M)	pH		
	5.8	7.4	8.0
0.05		X	
0.15	X	X	X
0.2		X	

prepared by stirring excess HAP in a 0.15 M NaCl (pH 7.4) solution, maintaining pH. After 12–24 h, the undissolved HAP was filtered (0.22 μ m, Isopore, Millipore). LRAP (16.8 mg) was then dissolved into 50 mL of SCP (326 μ g/mL), and the pH was adjusted to 7.4. For solutions with a different pH, the same procedure was followed, but the initial pH was adjusted to either 5.8 or 8.0. For solutions with different ionic strength, the same procedure was followed, but the NaCl concentration was adjusted to obtain the desired ionic strength (0.05 or 0.2 M).

Protein Adsorption to HAP. HAP was prepared for protein adsorption by washing 54.3 mg of HAP three times with 10 mL of SCP immediately before adding it to one of the above protein solutions. Upon addition of the protein solution, the mixture was stirred for 3 h at room temperature to allow binding. The mixture was centrifuged, and the LRAP–HAP complex was washed three times with 5 mL of SCP to remove nonspecifically bound protein. The amount of protein bound was determined by measuring the change in concentration before and after binding and for each wash using ultraviolet absorbance measurements ($\lambda = 277$ nm).

The prepared sample was packed into the NMR rotor by first transferring it to a 1 mL pipet tip in which the tip end was sealed. The tip was centrifuged for 10 min at 12 000 rpm to remove residual liquid, resulting in a tightly packed hydrated LRAP–HAP complex. The sealed end was then cut open, and the pellet was transferred to a 5 mm NMR rotor using a centrifuge. The rotor was spun in the probe at 6–7 kHz to remove the excess water, resulting in a >100% hydrated, surface bound sample. A thin layer of parafilm or a rubber disk was positioned before the end-cap to keep the sample fully hydrated during NMR data collection.

Protein off the Surface. To prepare protein samples off the surface, 20 mg of protein was dissolved in 1 mL of SCP and diluted to 20 mL with water, and the pH was adjusted to 7.4. This was frozen and lyophilized, and the entirety of the sample was packed into an NMR rotor.

NMR Experiments. NMR experiments were conducted on a three-channel Chemagnetics Infinity spectrometer (Chemagnetics, Fort Collins, CO) with an Oxford 7.05 T ($\nu_0(^1\text{H}) = 300$ MHz) wide-bore magnet, operating at resonance frequencies of $\nu_0(^{13}\text{C}) = 75.78$ MHz and $\nu_0(^{15}\text{N}) = 30.54$ MHz. For chemical shift and Herzfeld–Berger (HB)²⁷ analysis measurements, a double-resonance HX magic-angle spinning (MAS), variable temperature Chemagnetics probe was used. For REDOR measurements, a triple-resonance HXY MAS, variable-temperature Chemagnetics probe was used. Temperatures in the rotor were calibrated using $^{207}\text{Pb}(\text{NO}_3)_2$.²⁸ Chemical shifts, which reflect differences in the absorption frequency depending on the electronic environment around a given nucleus, were referenced to the adamantane CH peak at 40.26 ppm,²⁹ which was referenced to 2,2-dimethyl-2-silapentane-5-sulfonate (DSS).

Deconvolution of the 1D spectra was performed with Dmfit.³⁰

Dynamics. Proton-decoupled ^{13}C cross-polarization magic-angle spinning NMR spectra were acquired with a spinning speed of 1.5 kHz. To allow direct intensity comparisons between the hydrated sample at room temperature (23 °C) and at –45 °C, 28 672 scans were taken for each sample. Carbon chemical shift tensor (CSA) parameters were extracted using HB analysis. Only chemical shifts are reported for K²⁴ samples due to overlapping resonances rendering HB analysis unreliable.

REDOR. XY8 phase cycling was used on both observe (^{13}C) and dephasing channels (^{15}N or ^{31}P) for REDOR experiments.^{31,32} For all REDOR experiments, 180° pulses of 13.0–15.0 μ s were used for both the observe and dephasing nuclei with a 65 kHz TPPM decoupling field³³ during the recoupling and acquisition periods. Both $^{13}\text{C}\{^{15}\text{N}\}$ and $^{13}\text{C}\{^{31}\text{P}\}$ REDOR data were obtained for each sample preparation condition for L¹⁵V¹⁹(+P) and V¹⁹L²³(+P). REDOR data were also collected for several other samples, shown in Table 3, chosen based on a significant measured difference in chemical shift for a given sample compared to the chemical shift for either the standard condition or the phosphorylated protein. Data were acquired at –80 °C to eliminate contributions due to motion and at a spinning speed of 4 kHz. For $^{13}\text{C}\{^{15}\text{N}\}$ REDOR, dephasing points were collected for L¹⁵V¹⁹(+P), V¹⁹L²³(+P), and K²⁴S²⁸(+P) at 8, 24, 40, 56, 72, 88, 104, 128, and 152 rotor periods, where the two longest dephasing points, 128 and 152, were acquired to provide added confidence for longer measured distances. For L¹⁵V¹⁹(–P) and V¹⁹L²³(–P), a reduced set of data were collected, with points at 8, 40, 72, 104, 128, and 152 rotor cycles. 4096–8192 scans were taken for 8, 24, and 40 rotor periods, 8192–10 240 scans for 56, 72, and 88 rotor periods, and 16 384–20 480 scans for 128 and 152 rotor periods. For $^{13}\text{C}\{^{31}\text{P}\}$ REDOR, dephasing points were collected for L¹⁵V¹⁹(+P), V¹⁹L²³(+P), and K²⁴S²⁸(+P) at 8, 24, 40, 56, 72, 88, and 104, with a reduced set collected for L¹⁵V¹⁹(–P) and V¹⁹L²³(–P), with points at 8, 40, 72, and 104 rotor periods. 4096 scans were taken for 8, 24, 40, and 56 rotor periods, and 8192–16 384 scans were taken for 72, 88, and 104 rotor periods. All data were collected with a 1 s pulse delay. Each point in the dephasing curve represents the average of at least five repetitions. REDOR dephasing curves were corrected for the natural abundance background and were fit by simulations generated using SIMPSON.³⁴ The contribution of the natural abundance background (59 backbone carbonyls and 10 side-chain carbonyls, or 41% of the total signal) was corrected for in the REDOR simulations.

RESULTS

Binding Ratios of LRAP to HAP. The amount of LRAP bound onto the HAP crystal surface under each of the five conditions (Table 1) was determined using ultraviolet absorbance measurements ($\lambda = 277$ nm) of the protein solutions before and after binding. On average, non-phosphorylated variants had ~10% more protein bound to HAP than the phosphorylated variants, with values of 0.26 and 0.23 μ g/cm², respectively (the initial ratio of LRAP to HAP was 16.8 mg:54.3 mg), with little deviation as a function of condition (Table S1). Slightly lower binding was observed at pH = 8.0 for both phosphorylated and non-phosphorylated LRAP. Each of the reported values was averaged from 3 to 4 different preparations.

Chemical Shift Measurements. Changes in chemical shift indicate an alteration in the electronic environment around the nucleus. The electronic environment may be altered in many ways, and with proteins, it is commonly due to structural changes.^{35–37} Indeed, the deviation of backbone and $^{13}\text{C}\beta$ chemical shifts from random coil values is an established method for predicting secondary structure in proteins.³⁸ For example, relative to random coil values, backbone carbonyl carbon chemical shifts can change by 2–3 ppm as a function of changing secondary structure,^{35–37} moving downfield (larger ppm values) in α -helical regions and upfield in β -strand regions.

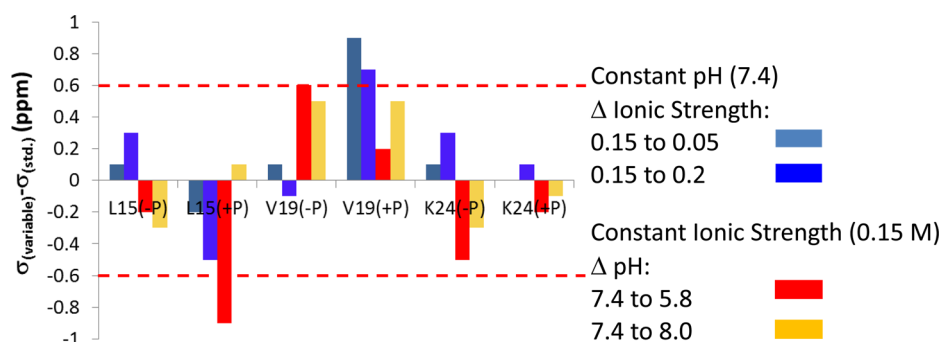


Figure 1. Changes in chemical shift as a function of preparation condition for the six samples vs the standard condition, for the $^{13}\text{C}'$ -labeled L^{15} , V^{19} , and K^{24} proteins. The most significant changes (extending outside of the red dashed lines) are observed for $\text{L}^{15}(+\text{P})$ and $\text{V}^{19}(+\text{P})$. Error bars on the $\Delta(\text{chemical shift})$ are ± 0.7 ppm. The values for K^{24} are based on the average chemical shifts.

The electronic environment may also be altered at the interface of protein binding, so chemical shift deviations could also be a result of protein–protein and/or protein–HAP interactions. Thus, chemical shift measurements are used as a relatively rapid (24 h) screening method for determining which conditions result in a change in the overall LRAP–HAP interaction.

The backbone carbonyl carbon ($^{13}\text{C}'$) chemical shifts at the three amino acid positions in the N-terminus (L^{15} , V^{19} and K^{24} , Table 1) were measured for each of the phosphorylated and unphosphorylated samples for each of the five different conditions. Typical spectra of the $^{13}\text{C}'$ resonances are shown in Figure S1, and the chemical shift data are tabulated in Table S2 and show small condition-dependent variations: L^{15} : 174.2–175.6 ppm, V^{19} : 173.9–175.2 ppm, and K^{24} : 178.3–179.1 ppm.

To investigate changes in the LRAP–HAP interface as a function of binding condition, chemical shift deviations relative to standard conditions (pH = 7.4 and IS = 0.15 M) were calculated; the results are shown in Figure 1 and Table S3. Of the 24 samples, four showed significant changes ($\Delta\delta > 0.6$ ppm): $\text{L}^{15}(+\text{P})$ at pH = 5.8, $\text{V}^{19}(+\text{P})$ at IS = 0.05 and 0.2 M, and for $\text{V}^{19}(-\text{P})$ at pH = 5.8. The error bars for the $\Delta(\text{chemical shift})$ are 0.7 ppm, indicative of the inherent error in determining chemical shifts for broad lines that are externally referenced. To avoid overlooking potential changes as a function of condition, we considered any ≥ 0.6 ppm as significant enough for the more quantitative REDOR study. Interestingly, the same condition does not consistently produce the same effect at each residue. For instance, changing the ionic strength from 0.15 to 0.2 with pH held constant (7.4) produced a large effect at $\text{V}^{19}(+\text{P})$, small effects at $\text{L}^{15}(-\text{P})$, $\text{L}^{15}(+\text{P})$, and $\text{K}^{24}(-\text{P})$, and almost no effect at $\text{V}^{19}(-\text{P})$ and $\text{K}^{24}(+\text{P})$. Changes outside of experimental error were not observed under any condition tested for $\text{L}^{15}(-\text{P})$, $\text{K}^{24}(-\text{P})$, or $\text{K}^{24}(+\text{P})$ compared to the standard condition.

Chemical shift differences were also characterized by determining perturbations as a function of phosphorylation. As seen in Figure 2 and Table S4, all of the $^{13}\text{C}'$ chemical shifts have a positive shift compared to the non-phosphorylated variant prepared under the same conditions. Significant chemical shift perturbations (≥ 0.6 ppm) are observed for three conditions at residue L^{15} and two conditions at residue V^{19} , with minimal changes observed at K^{24} .

Structure and Orientation. Chemical shift perturbations relative to our standard condition serve as a qualitative indicator of residues in the N-terminus which might alter the LRAP–HAP interface as a function of binding condition, by either a structural change or a change in protein orientation on the

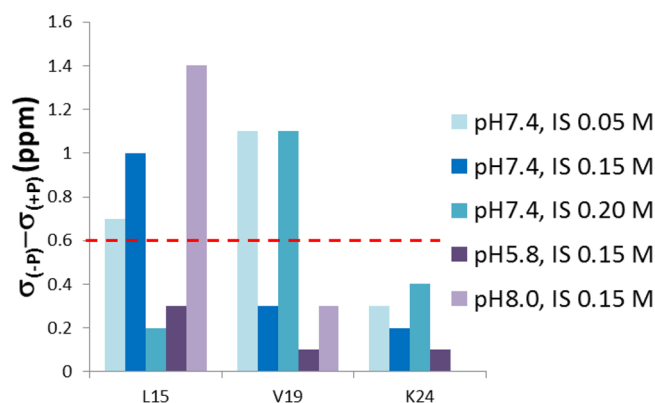


Figure 2. Differences in $^{13}\text{C}'$ chemical shift between phosphorylated and non-phosphorylated LRAP as a function of residue and condition. Phosphorylation produced significant chemical shift perturbations (above the red dashed line) for several conditions at L^{15} and V^{19} . Error bars on the $\Delta(\text{chemical shift})$ are ± 0.7 ppm. The values for K^{24} are based on the average chemical shifts.

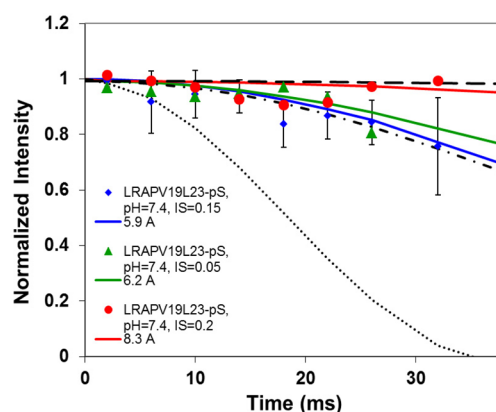


Figure 3. REDOR dephasing curves for $\text{V}^{19}\text{L}^{23}(+\text{P})$ as a function of ionic strength (pH = 7.4). The distance becomes measurably more extended, possibly to a β -sheet structure, at high ionic strength (red circles, 8.3 Å) when compared to standard conditions (blue diamonds, 5.9 Å), while the low ionic strength does not show a significant difference (green triangles, 6.2 Å). Error bars are only shown for one data set for clarity but are representative of the errors in each data set. The standard canonical structures are also shown: dots (α -helix), dot-dash (random coil), and dash (β -sheet).

surface. To establish the physical basis for the observed chemical shift perturbations, the LRAP samples with the most significant $^{13}\text{C}'$ chemical shift changes were investigated using

Table 3. Summary of the Data Obtained Using REDOR (New Data in Bold)^a

	pH 7.4, IS 0.05 M	pH 5.8, IS 0.15 M	pH 7.4, IS 0.15 M	pH 8.0, IS 0.15 M	pH 7.4, IS 0.2 M	off
¹³ C'– ¹⁵ N (secondary structure)						
L ¹⁵ V ¹⁹ (–P)	5.2 ± 0.5		4.9 ± 0.5 ^b	4.9 ± 0.5		5.0 ± 0.5 ^b
L ¹⁵ V ¹⁹ (+P)	4.6 ± 0.5	4.6 ± 0.5	4.8 ± 0.5 ^{b,c}	4.6 ± 0.5	4.4 ± 0.5	5.9 ± 0.5 ^b
V ¹⁹ L ²³ (–P)	6.1 ± 0.5		5.6 ± 0.5 ^b		6.3 ± 0.5	6.8 ± 1.0 ^b
V ¹⁹ L ²³ (+P)	6.2 ± 0.5	5.8 ± 0.5	5.9 ± 0.5 ^{b,c}	5.9 ± 0.5	8.3 ± 1.5	6.1 ± 0.5 ^b
K ²⁴ S ²⁸ (–P)			5.7 ± 0.5 ^b			4.5 ± 0.5 ^b
K ²⁴ S ²⁸ (+P)			4.8 ± 0.5			4.2 ± 0.5
¹³ C'– ³¹ P (backbone to HAP distance)						
L ¹⁵ (–P)	9.5 ± 1.0		9.0 ± 0.75 ^b	9.5 ± 1.0		
L ¹⁵ (+P)	5.4 ± 0.5 ^d	5.3 ± 0.5 ^d	5.3 ± 0.5 ^{b,d}	5.4 ± 0.5 ^d	5.1 ± 0.5 ^d	
V ¹⁹ (–P)	10.0 ± 1.0		9.0 ± 0.75 ^b		10.0 ± 1.0	
V ¹⁹ (+P)	7.2 ± 0.5	7.2 ± 0.5	7.0 ± 0.5 ^b	7.0 ± 0.5	7.0 ± 0.5	
K ²⁴ (–P)			9.0 ± 0.75 ^b			
K ²⁴ (+P)			7.5 ± 0.5			

^aTop: ¹³C–¹⁵N distances of L¹⁵V¹⁹(–P/+P), V¹⁹L²³(–P/+P), and K²⁴S²⁸(–P/+P) under selected conditions. Bottom: ¹³C–³¹P distances of L¹⁵(–P/+P), V¹⁹(–P/+P), and K²⁴S²⁸(–P/+P) to the surface of HAP under selected conditions. ^bIndicates distance measurements that were reported previously and are shown here for comparison. ^cIndicates data that is slightly modified from that previously reported due to the addition of extra dephasing points run here. ^dIndicates ¹³C–³¹P measurements that have a ³¹P nearby in the protein backbone, resulting in an overall shorter distance than what is really present between the protein backbone and HAP.

the solid-state NMR technique rotational echo double resonance (REDOR). REDOR utilizes the dipolar interaction between two isolated, isotopically labeled nuclei (e.g., ¹³C and ¹⁵N) to determine the structure of the protein in that region. The distance from ¹³C' in the backbone to the ³¹P in the surface is used to determine the distance of a particular residue from the surface and, consequently, the orientation of the protein with respect to HAP.

Structure. For structural determination, we introduce a carbonyl (¹³C') at the *i*th residue and an ¹⁵N at the *i* + 4 residue in the backbone of the protein. The distance measured between the two residues is characteristic of certain structures. For instance, a distance of 4.2 Å between these two spins is consistent with a perfect α-helical structure in this region of the protein. A β-sheet structure would give a distance of 10.6 Å, which is beyond the range that REDOR can accurately measure, providing a very clear distinction between these two extremes. The average distance that a random coil protein would experience is 5.8 Å, generated by taking an average of the dephasing curves at each of the distances between 4.2 and 10.6 Å in 0.1 Å increments. The REDOR dephasing curves for each type of structure are shown in Figure 3.

Because the largest chemical shift perturbations as a function of binding condition were predominantly observed for L¹⁵(+P) and V¹⁹(+P), each of the binding conditions for these two samples was investigated using REDOR. The data for all of the samples are tabulated in Table 3. The ¹³C{¹⁵N} REDOR dephasing curves for V¹⁹L²³(+P) at constant pH (7.4) and varying ionic strength (0.05, 0.15, and 0.2 M) are representative and are shown in Figure 3, with the experimental data represented by symbols and the fits shown as lines. Error bars were determined from at least five measurements, and the best-fit distances were determined by a χ² analysis on the dephasing curves compared to simulated curves. Dephasing curves for α-helical (dotted curve, 4.2 Å), β-sheet (dashed curve, 10.6 Å), and random coil (dotted-dashed curve, 5.8 Å) structures are also shown for comparison.

The structure of V¹⁹L²³(+P) does not change from that observed under standard conditions as a function of pH but does show variability as a function of ionic strength. This

change is slight when the ionic strength is lowered to 0.05 M, from 5.9 to 6.2 Å, and is significant at an ionic strength of 0.2 M, from 5.9 to 8.3 Å, where the measured distance changes to a more extended or β-sheet-like structure. Structural changes are also observed for V¹⁹L²³(–P) as a function of ionic strength, where both low and high ionic strengths result in a slight increase in distance (from 5.6 Å to 6.1 and 6.3 Å, respectively). It is also noteworthy that phosphorylation of V¹⁹L²³ results in a significant increase in distance, from 6.3 to 8.3 Å, at 0.2 M ionic strength. Extra dephasing points, 128 and 152 (or 38 ms), were run to confirm these long distances. The backbone distance, and consequently the structure, of L¹⁵V¹⁹(+P) and L¹⁵V¹⁹(–P) is unchanged within experimental error under all of the conditions studied. The distances of the same spin pairs under standard conditions were previously reported and are shown here for comparison.⁴

The structure of K²⁴S²⁸(–P) was previously reported both on and off HAP and was observed to unfold from a nearly perfect helix off the surface (4.5 Å) to a largely unstructured form on the surface (5.7 Å).⁴ In this work we investigated the phosphorylated variant, K²⁴S²⁸(+P), both off the surface and adsorbed to the surface using REDOR. Similar to the unphosphorylated variant, we observed a distance consistent with a perfect helix off the surface (4.2 Å), but in the phosphorylated case, it maintains a largely helical structure (4.8 Å) when bound to HAP under standard conditions (Figure 4 and Table 3).

The one-dimensional spectra of these samples provide interesting structural insights (Figure 5). Rather than existing as a broad symmetric Lorentzian peak as observed for the other residues (Figure S1), the ¹³C' resonance for the K²⁴ samples clearly consist of multiple, noncoincident resonances. This is the only residue for which this was observed, consistent with a unique structure or orientation at this residue in the protein. Because of the significant difference in spectra for the K²⁴S²⁸(+P) sample, the protein was synthesized two times and the sample under standard conditions prepared with each protein preparation; identical results were obtained in both cases. The spectrum of K²⁴S²⁸(+P) off the surface has two overlapping resonances, the largest of which is downfield (~179 ppm). In this case, the downfield chemical shift is

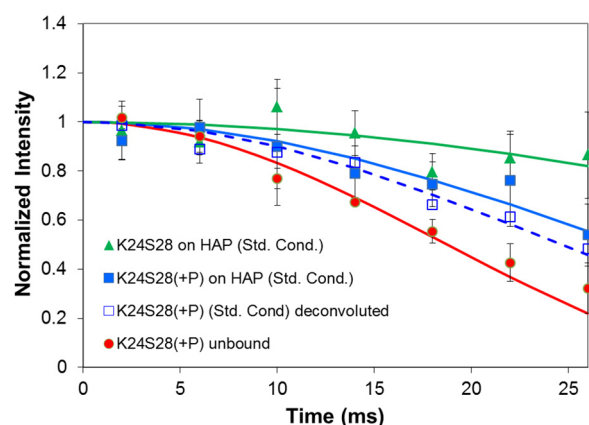


Figure 4. $^{13}\text{C}\{^{15}\text{N}\}$ REDOR show that $\text{K}^{24}\text{S}^{28}$ changes structure as a function of binding, and as a function of phosphorylation. The solid lines are the best fit distances: (red 4.2 Å, blue 4.8 Å, and green 5.7 Å). Binding transforms the phosphorylated peptide from a perfect helix to a combination of two structures, helix and either random coil or β -sheet. Dephosphorylation extends the structure further and is consistent with a combination of random coil, helix and β -sheet.⁴ Data generated from deconvolution are also shown (open blue squares) with the dashed blue line fit of 4.6 Å.

expected for, and consistent with, the helical structure measured using REDOR. The upfield resonance (~ 174 ppm) in this case is due to the natural abundance backbone amide resonances. When $\text{K}^{24}\text{S}^{28}(+P)$ is bound to the surface, the intensity of the downfield (helical) resonance is reduced, and a third resonance (~ 175.5 ppm), in between the resonances corresponding to a helical structure and the unlabeled backbone amides, increases. The deconvolutions for each sample are summarized in Table S5. This strongly suggests that LRAP has two unique structures in this region: one helical ($\sim 85\%$) and one more random coil or β -sheet in structure based on the upfield shift.³⁵ When the un-phosphorylated variant ($\text{K}^{24}\text{S}^{28}(-P)$) is bound to HAP, the distribution is further shifted to the more extended structure, as evidenced by the shift in relative intensity (Figure 5), with the contribution to the helical component diminished to $\sim 45\%$.

Reevaluating the REDOR dephasing curves to include two unique structures for the bound samples of $\text{K}^{24}\text{S}^{28}(-P)$ and $\text{K}^{24}\text{S}^{28}(+P)$ offers several interpretations that would be consistent with the data. A combination of 50% helix (4.2 Å) and 50% β -sheet (10.6 Å) or 40% helix and 60% random coil (5.8 Å) fits the $\text{K}^{24}\text{S}^{28}(+P)$ data equally as well as a single distance of 4.8 Å. The estimate of 50% helix is lower than that estimated by the deconvoluted area of the helical component in the 1D spectrum ($\sim 85\%$) and could be due to a loose helical structure rather than the tight helical structure (4.2 Å) assumed for the fitting. The $\text{K}^{24}\text{S}^{28}(-P)$ data is fit equally well to a random coil structure, or a mixture of 25% helix and 75% β -sheet. Since there are two distinct resonances, it is unlikely that it is best described only by a random coil which would give just one resonance. The complexity of the lineshape suggests that an even more complex mixture containing some helix, some random coil and some β -sheet may be most consistent with the data.

To provide further insight into the structure, we deconvoluted each point in the dephasing curve of $\text{K}^{24}\text{S}^{28}(+P)$ for pH = 7.4, IS = 0.15 M into two peaks, the maximum that was appropriate given the resolution of the REDOR resonances (Figure S2). This results in a peak at the

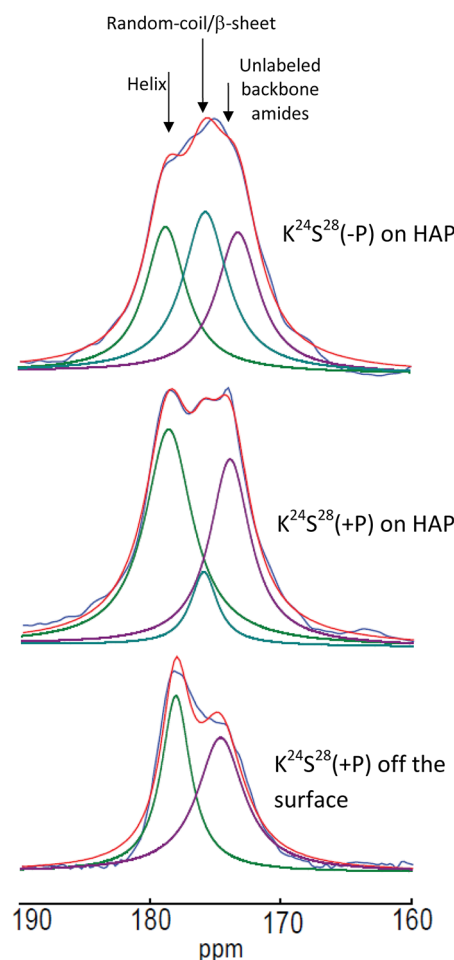


Figure 5. Comparison of the $^{13}\text{C}'$ chemical shifts for $\text{K}^{24}\text{S}^{28}$ at 23 °C. Bottom: $\text{K}^{24}\text{S}^{28}(+P)$ lyophilized from solution. Middle: $\text{K}^{24}\text{S}^{28}(+P)$ bound to HAP under standard conditions, pH = 7.4, IS = 0.15 M. Top: $\text{K}^{24}\text{S}^{28}(-P)$ bound to HAP under standard conditions, pH = 7.4, IS = 0.15 M. Dark blue: experimental data; red: simulated fit; green, pale blue and maroon: deconvoluted components.

chemical shift of the helical resonance and one that is composed of the natural abundance backbone resonances and the random coil/ β -sheet resonance. The helical component has a distance of 4.6 Å, shorter and more helical in structure than that determined for the composite resonance (4.8 Å), consistent with our interpretation that this resonance represents a helical component (Figure 4). The deviation from the distance expected for a pure helix (4.2 Å) could be due to a loose helical structure, imperfect deconvolution, or unaccounted for background contribution. The interpretation of a loose helix is consistent with the deviations observed with REDOR in evaluating the composite peak and provides the most consistent explanation for all of the data. While the exact structure is still not entirely established, this analysis emphasizes the power of considering both chemical shift and dipolar recoupling in evaluating structural data to provide deeper insight.

Orientation. In order to understand how pH, ionic strength, and phosphorylation affect the orientation of LRAP on HAP, solid-state NMR $^{13}\text{C}\{^{31}\text{P}\}$ REDOR experiments were also carried out to determine the distance between one of the three backbone $^{13}\text{C}'$ -labeled residues (L^{15} , V^{19} or K^{24}) and the closest ^{31}P on the surface of HAP. The $^{13}\text{C}-^{31}\text{P}$ distances are listed in

Table 3 and show that the residue–HAP distances do not change significantly for $L^{15}(+P/-P)$ or $V^{19}(+P/-P)$ with solution conditions.

Both L^{15} and V^{19} were previously found to move closer to the surface upon phosphorylation. In this work, it was found that K^{24} , eight residues from the pS^{16} , is also closer to the HAP surface upon phosphorylation with the average distance decreasing from 9.0 Å in the un-phosphorylated variant to 7.5 Å in the phosphorylated derivative (Table 3). The $^{13}C\{^{31}P\}$ REDOR dephasing curves for $K^{24}(-P)$ and $K^{24}(+P)$ under standard conditions (pH = 7.4, IS = 0.15 M) are shown in Figure 6.

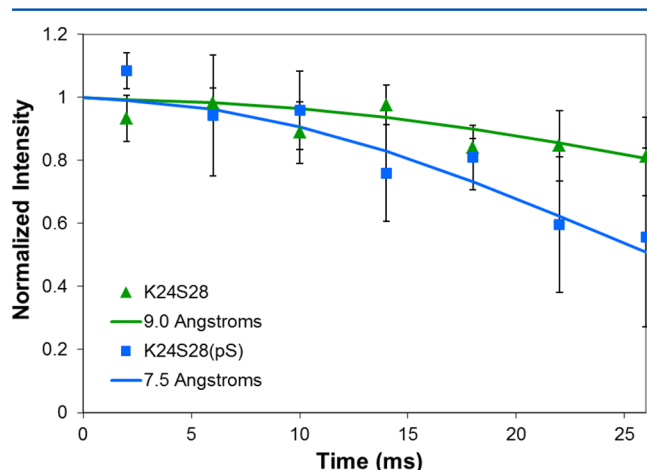


Figure 6. $^{13}C\{^{31}P\}$ REDOR dephasing curves for K^{24} and $K^{24}(pS)$ bound to HAP under standard conditions showing that phosphorylation results in a closer association of K^{24} with the surface.

Dynamics. One-dimensional $^{13}C\{^1H\}$ cross-polarization magic-angle spinning NMR spectra were obtained for each of

the LRAP–HAP complexes at two different temperatures (23 and $-45^\circ C$), but otherwise identical experimental conditions, in order to gain information on the dynamics of LRAP when it is bound to the surface as a function of solution condition. In a hydrated environment, little motion is expected at sites strongly associated with HAP, while significant motion is expected for weakly bound sites.^{4,6,7} A representative example of the data is shown in Figure 7 for $L^{15}(-P)$ as a function of the series of solution conditions. Each of the samples was investigated at low temperature (Figure 7, left) and at room temperature (Figure 7, right). In each case, LRAP shows an increase of motion at room temperature compared to the frozen state. This is evidenced by the decreased signal-to-noise observed for the room temperature spectra, particularly evident at pH = 5.8 for $L^{15}(-P)$. The loss of signal intensity is due to inefficient cross-polarization and proton decoupling.

Dynamic information can also be extracted from the spinning sideband pattern in the one-dimensional spectra. Both the span (Ω) of the chemical shift anisotropy and the relative intensities of the resonances (η) are related to dynamic processes, and these values are reported for each sample in Table S2. Using a Herzfeld–Berger (HB) analysis, the span, $\Omega = |\sigma_{11} - \sigma_{33}|$, of all of the samples that were measurable decreases moderately from ~ 140 ppm at $-45^\circ C$ to ~ 100 to ~ 130 ppm at $23^\circ C$. The η values range from 0.5 to 0.8 and are evident in the spectra, where the isotropic peak, indicated with an arrow, increases moderately in intensity relative to the other spinning side bands, suggesting that none of the regions under the conditions studied have a highly stable interaction with the surface. The lack of a dramatic change in the chemical shift anisotropy suggests that the motion is restricted.

The one-dimensional spectra at $23^\circ C$ for all of the preparation conditions of the LRAP–HAP complexes studied

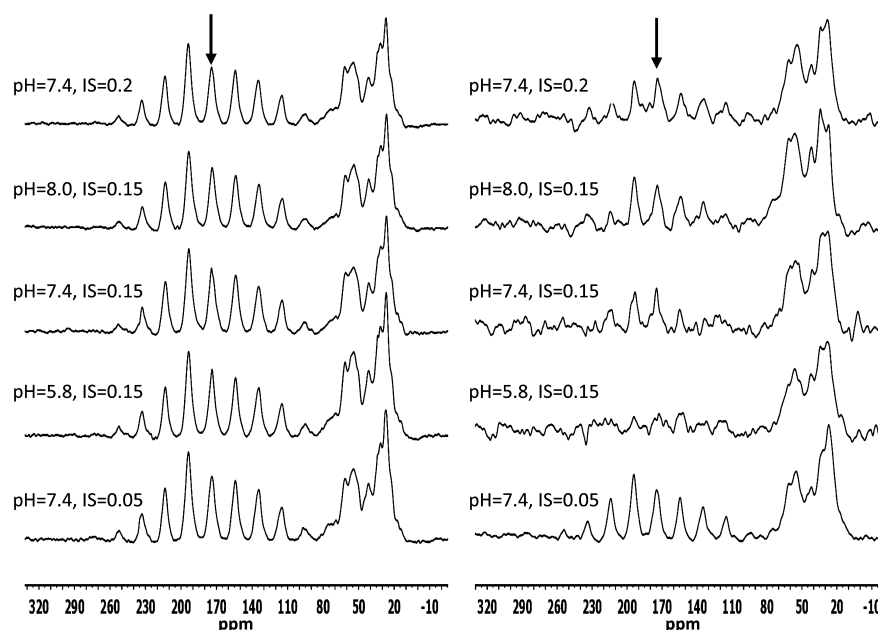


Figure 7. One-dimensional spectra shown for $L^{15}(-P)$ under each condition, as indicated. Left, $-45^\circ C$; right, $23^\circ C$. Each sample has reduced signal-to-noise compared to the spectra when taken under frozen conditions, indicating mobility. The spectra at pH = 7.4, IS = 0.2 and 0.15 M also show an increased intensity in the isotropic peak (marked with an arrow) relative to the spinning side bands, suggesting even more mobility under these conditions; however, in all cases, the data suggest that the mobility is restricted.

show similar features, i.e., a loss of signal-to-noise, a slight decrease of Ω , with no change or a relatively small change in η compared to the spectra at -45°C , the frozen state. For nearly every binding condition for $\text{L}^{15}(+\text{P})$, the signal-to-noise decreased so significantly that obtaining good HB analyses (values for Ω and η) was not possible, suggestive of more motion at these two residues in the protein. Conditions for other labeling schemes also had poor signal-to-noise preventing a HB analysis, but not for a consistent binding condition or phosphorylation state; therefore, it does not suggest a specific trend in the intensity of the dynamics and how it may influence function. The CSA parameters for $\text{K}^{24}(-\text{P})$ and $\text{K}^{24}(+\text{P})$ were not determined due to multiple overlapping peaks, discussed *vide infra*, although decreased signal-to-noise was also observed for these samples, particularly $\text{K}^{24}(-\text{P})$ which had almost no remaining signal at 23°C under the analysis conditions for any binding condition.

DISCUSSION

During enamel formation, environmental conditions change significantly, including the ionic strength, pH, surface type, and protein concentration.^{12–14,39,40} The protein phosphorylation state may also change during enamel formation. The role of each variable is unclear, but they may result in modified protein structure or alter the protein–mineral interface, thereby controlling the mechanism of enamel development. To examine this possibility, three of these variables, the ionic strength, phosphorylation state, and the pH, were investigated to evaluate their impact on the secondary structure, orientation, and dynamics of LRAP bound to HAP.

The Role of Solution Conditions in Modulating the Interface of LRAP and HAP. Under all of the pH and ionic strength conditions studied, very few changes in structure, orientation, or dynamics were observed based on both chemical shift and REDOR data, suggesting a very stable LRAP–HAP interaction overall. Under every condition and in each region, restricted mobility is observed, implying that each region is interacting with HAP but that the interaction is not rigid. The increased mobility observed for $\text{L}^{15}(+\text{P})$ under all conditions may be indicative of an important change in those regions to assist function as the solution environment around enamel changes.

The REDOR evaluation of the structure and orientation of the full set of conditions for the region encompassing L^{15} to V^{19} in $\text{LRAP}(+\text{P})$ shows no change as a function of sample preparation condition outside of experimental error, and are all found to contain significant helical content in this region, with a distance of $\sim 4.5\text{--}5\text{ \AA}$, and oriented close to the surface. The stable structure and orientation as a function of pH and ionic strength are unexpected since protein secondary structure is often observed to be sensitive to pH and ionic strength,^{41–44} and a change in secondary structure would have the potential to change the orientation of the protein. This stability may suggest an important role for this region of the protein, either in interacting with HAP or in positioning it to interact with other proteins.

The region from V^{19} to L^{23} in $\text{LRAP}(+\text{P})$ was also investigated with REDOR under the full set of conditions. The orientation of this region with respect to HAP did not change under any condition, nor did the structure in this region change as a function of pH. However, the structure in this region did change as a function of ionic strength, from largely random coil under standard conditions to a more extended or

β -sheet structure at higher ionic strengths (0.2 M). In comparing the REDOR results with the chemical shift data, the $\text{V}^{19}\text{L}^{23}(+\text{P})$ samples also had a perturbed chemical shift as a function of ionic strength, suggesting that the change in chemical shift is at least partially due to the change in secondary structure.

Recent reports have shown a connection between ionic strength and the ability of phosphorylated amelogenin to form chainlike structures.¹⁸ The changes observed here between ionic strength and the structure of the $\text{V}^{19}\text{L}^{23}(+\text{P})$ (Table 3) may be related to the previously reported observation. The structural flexibility in this region as the ionic strength fluctuates may be connected to a role in regulating crystal growth as the enamel environment changes.

Previous reports on the solution state structure of amelogenin indicate a sensitivity to pH changes ($2^{19,20}$ and 3.8^{21} vs 5.5^{22}). Specifically, at higher pH values, increased structure was observed. Two regions in the N-terminus, $\text{S}^9\text{--V}^{19}$ and $\text{K}^{24}\text{--I}^{30}$, were suggested to be structured at pH 5.5,²² while they were not structured at lower pH values.^{19–21} The surface bound sample was insensitive to pH, and additionally, our data suggest a mixture of helical and unstructured or β -sheet regions in the N-terminus for the surface bound sample, consistent with the structurally dynamic nature of this protein.

The Role of Phosphorylation in Modulating the LRAP–HAP Interface. Under standard conditions (pH 7.4, $\text{IS} = 0.15\text{ M}$), the structure in the region from L^{15} to V^{19} and V^{19} to L^{23} did not change upon phosphorylation. However, changes in structure were observed in the region from K^{24} to S^{28} under standard conditions as a function of phosphorylation, shifting from a largely random coil structure to a structure with significant helical content. The observed structural switching as a function of phosphorylation may be indicative of an important *in vivo* mechanism. Following phosphorylation, K^{24} was also observed to be closer to the HAP surface, an observation that was noted for L^{15} and V^{19} , but was unexpected here due to the distance from pS^{16} .

In addition to the quantitative distance measurements, in general, larger chemical shift differences were observed as a function of phosphorylation for each of the binding conditions than as a function of the binding condition alone (Figure 2 and Table S4). REDOR investigations revealed that only $\text{V}^{19}\text{L}^{23}$ at high ionic strength shows a significant change in secondary structure upon phosphorylation, further implicating this region to have a potential functional importance *in vivo*. Phosphorylation has been observed to have an effect on the amount of LRAP bound,⁴ nanosphere formation,⁹ the structure when interacting with calcium,²³ nanosphere chain formation,¹⁸ and ACP transformation to HAP.⁴⁵ This work provides evidence that the molecular level interactions also change as a function of phosphorylation and may be related to the macroscopic observations.

The Special Nature of K24: Implications *in Vivo*. The changes in $\text{K}^{24}\text{S}^{28}$ as a function of phosphorylation are interesting. This region is 8–12 residues from the phosphoserine, yet the distance from the surface was impacted as much as it was for V^{19} , only three residues from the phosphoserine. Additionally, two unique structures are observed at $\text{K}^{24}\text{S}^{28}(+\text{P})$, consistent with 40–50% helix with the remainder random coil or β -sheet, respectively. The un-phosphorylated variant, $\text{K}^{24}\text{S}^{28}(-\text{P})$, contains only 25–30% helix. This significant change in structure suggests that there may be a structural switching mechanism occurring upon dephosphorylation.

Preparation under different solution binding conditions alter the relative amounts of the two structural motifs, further pointing to a sensitive structural region that may have an important role in regulating mineralization. Solution state data of an N-terminal fragment of non-phosphorylated amelogenin reported previously indicate that there is a turn between residues V¹⁹ and K²⁴,²² consistent with the data shown here that K²⁴ is at a structurally flexible location.

These observations could point to a unique functional role for this region upon de-phosphorylation. There are phosphatases present in the enamel environment, lending support to this interpretation.⁴⁶ It has also been recently observed that amorphous calcium phosphate (ACP) is transformed to HAP but that pS¹⁶ in both amelogenin and LRAP stabilizes ACP longer than the non-phosphorylated variant.^{40,45} The mechanism by which the transformation is triggered is unclear, but it is likely that the transformation is due to a change in the interaction of amelogenins with HAP as enamel matures, and structural changes in the region of K²⁴ as a function of dephosphorylation may be associated with this transformation. Investigations as a function of surface type, protein concentration, or other variable conditions found in the enamel milieu could provide more insight into this potentially important region of the protein.

SUMMARY

The N-terminus of the amelogenin protein, LRAP, was found to have a reasonably stable interfacial interaction with HAP as a function of changes in ionic strength and pH during binding. Very little structural or orientation variation was observed from L¹⁵ to L²³, with the exception that V¹⁹L²³(+P) becomes more extended with higher ionic strength. Phosphorylation does modulate both the structure and the interaction of the N-terminus with HAP, particularly at residue K²⁴ which undergoes a large structure and orientation change. This observation could be relevant to the proteins function *in vivo*, where dephosphorylation or changes in ionic strength may trigger a structural change to initiate a different growth phase of HAP. Increased mobility as a function of phosphorylation seen for L¹⁵(+P) may also contribute to this function. Studies investigating other conditions found to vary in enamel, as well as investigating the highly charged region in the C-terminus of LRAP, should provide additional insight into the amelogenin–HAP interface and how it changes during enamel development.

ASSOCIATED CONTENT

Supporting Information

Table of LRAP binding ratios; table of chemical shifts and CSA parameters; table of chemical shift differences between the variable conditions and the standard condition; table of chemical shift differences between phosphorylated and non-phosphorylated LRAP; figure showing typical 1D spectra of the carbonyl carbon; figure showing the deconvolution of several points in the REDOR dephasing curve of K²⁴S²⁸(+P). This material is available free of charge via the Internet at <http://pubs.acs.org>.

AUTHOR INFORMATION

Corresponding Author

*E-mail wendy.shaw@pnnl.gov; Ph 509-375-5922.

Funding

Funding was provided by NIH-NIDCR Grant DE-015347.

Notes

The authors declare no competing financial interest.

ACKNOWLEDGMENTS

This research was supported by NIH-NIDCR Grant DE-015347. The research was performed at the Pacific Northwest National Laboratory (PNNL), a facility operated by Battelle for the U.S. Department of Energy.

REFERENCES

- (1) Simmer, J. P., and Fincham, A. G. (1995) Molecular mechanisms of dental enamel formation. *Crit. Rev. Oral Biol. Med.* 6, 84–108.
- (2) Fincham, A. G., Moradian-Oldak, J., and Simmer, J. P. (1999) The structural biology of the developing dental enamel matrix. *J. Struct. Biol.* 136, 270–299.
- (3) Moradian-Oldak, J., Tan, J., and Fincham, A. G. (1998) Interaction of amelogenin with hydroxyapatite crystals: an adherence effect through amelogenin molecular self-association. *Biopolymers* 46, 225–238.
- (4) Masica, D. L., Gray, J. J., and Shaw, W. J. (2011) Partial high-resolution structure of phosphorylated and non-phosphorylated leucine-rich amelogenin protein adsorbed to hydroxyapatite. *J. Phys. Chem. C* 115, 13775–13785.
- (5) Shaw, W. J., Campbell, A. A., Paine, M. L., and Snead, M. L. (2004) The COOH terminus of the amelogenin, LRAP, is oriented next to the hydroxyapatite surface. *J. Biol. Chem.* 279, 40263–40266.
- (6) Shaw, W. J., and Ferris, K. (2008) Structure, orientation, and dynamics of the C-terminal hexapeptide of LRAP determined using solid-state NMR. *J. Phys. Chem. B* 112, 16975–16981.
- (7) Shaw, W. J., Ferris, K., Tarasevich, B., and Larson, J. L. (2008) The structure and orientation of the C-terminus of LRAP. *Biophys. J.* 94, 3247–3257.
- (8) Moradian-Oldak, J., Jimenez, I., Maltby, D., and Fincham, A. G. (2001) Controlled proteolysis of amelogenins reveals exposure of both carboxy- and amino terminal regions. *Biopolymers* 58, 606–616.
- (9) Moradian-Oldak, J., Bouropoulos, N., Wang, L., and Gharakhanian, N. (2002) Analysis of self-assembly and apatite binding properties of amelogenin protein lacking the hydrophilic C-terminal. *Matrix Biol.* 21, 197–205.
- (10) Aoba, T., Moreno, E. C., Kresak, M., and Tanabe, T. (1989) Possible roles of partial sequences at N- and C-termini of amelogenin in protein-enamel mineral interaction. *J. Dent. Res.* 68, 1331–1336.
- (11) Aoba, T., Fukae, M., Tanabe, T., Shimizu, M., and Moreno, E. C. (1987) Selective adsorption of porcine-amelogenins onto hydroxyapatite and their inhibitory activity on hydroxyapatite growth in supersaturated solutions. *Calcif. Tissue Int.* 41, 281–289.
- (12) Moradian-Oldak, J., Leung, W., and Fincham, A. G. (1998) Temperature and pH-dependent supramolecular self-assembly of amelogenin molecules: A dynamic light-scattering analysis. *J. Struct. Biol.* 122, 320–327.
- (13) Sasaki, S., Takagi, T., and Suzuki, M. (1991) Cyclical changes in pH in bovine developing enamel as sequential bands. *Arch. Oral Biol.* 36, 227–231.
- (14) Robinson, C., Kirkham, J., Brookes, S. J., Bonass, W. A., and Shore, R. C. (1995) The chemistry of enamel development. *Int. J. Dev. Biol.* 39, 145–152.
- (15) Aichmayer, B., Wiedemann-Bidlack, F. B., Gilow, C., Simmer, J. P., Yamakoshi, Y., Emmerling, F., Margolis, H. C., and Fratzl, P. (2010) Amelogenin nanoparticles in suspension: deviations from spherical shape and pH-dependent aggregation. *Biomacromolecules* 11, 369–376.
- (16) Moradian-Oldak, J. (2001) Amelogenins: assembly, processing and control of crystal morphology. *Matrix Biol.* 20, 293–305.
- (17) Moradianoldak, J., Simmer, J. P., Lau, E. C., Sarte, P. E., Slavkin, H. C., and Fincham, A. G. (1994) Detection of monodisperse

aggregates of a recombinant amelogenin by dynamic light-scattering. *Biopolymers* 34, 1339–1347.

(18) Wiedemann-Bidlack, F. B., Kwak, S. Y., Beniash, E., Yamakoshi, Y., Simmer, J. P., and Margolis, H. C. (2011) Effects of phosphorylation on the self-assembly of native full-length porcine amelogenin and its regulation of calcium phosphate formation in vitro. *J. Struct. Biol.* 173, 250–260.

(19) Buchko, G. W., Tarasevich, B. J., Bekhazi, J., Snead, M. L., and Shaw, W. J. (2008) A solution NMR investigation into the early events of amelogenin nanosphere self-assembly initiated with sodium chloride or calcium chloride. *Biochemistry* 47, 13215–13222.

(20) Buchko, G. W., Tarasevich, B. J., Roberts, J., Snead, M. L., and Shaw, W. J. (2010) A solution NMR investigation into the murine amelogenin splice-variant LRAP (leucine-rich amelogenin protein). *Biochim. Biophys. Acta, Proteins Proteomics* 1804, 1768–1774.

(21) Delak, K., Harcup, C., Lakshminarayanan, R., Sun, Z., Fan, Y., Moradian-Oldak, J., and Evans, J. S. (2009) The tooth enamel protein, procine amelogenin, is an intrinsically disordered protein with an extended molecular configuration in the monomeric form. *Biochemistry* 48, 2272–2281.

(22) Zhang, X., Ramirez, B. E., Liao, X., and Diekwisch, T. G. H. (2011) Amelogenin supramolecular assembly in nanospheres defined by a complex helix-coil-PPII helix 3D-structure. *PLoS One* 6, e24952.

(23) Le Norcy, E., Kwak, S. Y., Allaire, M., Fratzl, P., Yamakoshi, Y., Simmer, J. P., and Margolis, H. C. (2011) Effect of phosphorylation on the interaction of calcium with leucine-rich amelogenin peptide. *Eur. J. Oral Sci.* 119 (Suppl 1), 97–102.

(24) Carpino, L. A., and Han, G. Y. (1972) 9-Fluorenylmethoxycarbonyl amino-protecting group. *J. Org. Chem.* 37, 3404–3409.

(25) Wiek, S., Masiukiewicz, E., and Rzeszotarska, B. (1999) A large scale synthesis of mono- and di-urethane derivatives of lysine. *Chem. Pharm. Bull. (Tokyo)* 47, 1489–1490.

(26) Ebrahimpour, A., Johnsson, M., Richardson, C. F., and Nancollas, G. H. (1993) The characterization of hydroxyapatite preparations. *J. Colloid Interface Sci.* 159, 158–163.

(27) Herzfeld, J., and Berger, A. E. (1980) Sideband intensities in NMR-spectra of samples spinning at the magic angle. *J. Chem. Phys.* 73, 6021–6030.

(28) Bielecki, A., and Burum, D. P. (1995) Temperature-dependence of Pb-207 MAS spectra of solid lead nitrate - an accurate, sensitive thermometer for variable-temperature MAS. *J. Magn. Reson., Ser. A* 116, 215–220.

(29) Wishart, D. S., Bigam, C. G., Yao, J., Abildgaard, F., Dyson, H. J., Oldfield, E., Markley, J. L., and Sykes, B. D. (1995) H-1, C-13 and N-15 chemical-shift referencing in biomolecular NMR. *J. Biomol. NMR* 6, 135–140.

(30) Massiot, D., Fayon, F., Capron, M., King, I., Le Calve, S., Alonso, B., Durand, J. O., Bujoli, B., Gan, Z., and Hoatson, G. (2002) Modelling one and two-dimensional solid-state NMR spectra. *Magn. Reson. Chem.* 40, 70–76.

(31) Gullion, T., and Schaefer, J. (1989) Rotational-echo double-resonance NMR. *J. Magn. Reson.* 81, 196–200.

(32) Gullion, T., and Schaefer, J. (1991) Elimination of resonance offset effects in rotational-echo, double-resonance NMR. *J. Magn. Reson.* 92, 439–442.

(33) Bennett, A. E., Rienstra, C. M., Auger, M., Lakshmi, K. V., and Griffin, R. G. (1995) Heteronuclear decoupling in rotating solids. *J. Chem. Phys.* 103, 6951–6958.

(34) Bak, M., Rasmussen, J. T., and Nielsen, N. C. (2000) SIMPSON: A general simulation program for solid-state NMR spectroscopy. *J. Magn. Reson.* 147, 296–330.

(35) Szilagyi, L. (1995) Chemical-shifts in proteins come of age. *Prog. Nucl. Magn. Reson. Spectrosc.* 27, 325–443.

(36) Wishart, D. S., Sykes, B. D., and Richards, F. M. (1991) Relationship between nuclear-magnetic-resonance chemical-shift and protein secondary structure. *J. Mol. Biol.* 222, 311–333.

(37) Wishart, D. S., Bigam, C. G., Holm, A., Hodges, R. S., and Sykes, B. D. (1995) ¹H, ¹³C and ¹⁵N random coil NMR chemical shifts of

the common amino acids. I. Investigations of nearest-neighbor effects. *J. Biomol. NMR* 5, 67–81.

(38) Wuthrich, K. (1986) *NMR of Proteins and Nucleic Acids*, John Wiley and Sons, New York.

(39) Aoba, T., and Moreno, E. C. (1987) The enamel fluid in the early secretory stage of porcine amelogenesis: chemical composition and saturation with respect to enamel mineral. *Calcif. Tissue Int.* 41, 86–94.

(40) Le Norcy, E., Kwak, S. Y., Wiedemann-Bidlack, F. B., Beniash, E., Yamakoshi, Y., Simmer, J. P., and Margolis, H. C. (2011) Leucine-rich amelogenin peptides regulate mineralization in vitro. *J. Dent. Res.* 90, 1091–1097.

(41) Bader, M. W., Sanowar, S., Daley, M. E., Schneider, A. R., Cho, U., Xu, W., Klevit, R. E., Moual, H. L., and Miller, S. I. (2005) Recognition of antimicrobial peptides by a bacterial sensor kinase. *Cell* 122, 461–472.

(42) DeGrado, W. F., and Lear, J. D. (1985) Induction of peptide conformation at apolar/water interfaces. I. A study with model peptides of defined hydrophobic periodicity. *J. Am. Chem. Soc.* 107, 7684–7689.

(43) Prost, L. R., Daley, M. E., Bader, M. W., Klevit, R. E., and Miller, S. I. (2008) The PhoQ histidine kinases of Salmonella and Pseudomonas spp. are structurally and functionally different: evidence that pH and antimicrobial peptide sensing contribute to mammalian pathogenesis. *Mol. Microbiol.* 69, 503–519.

(44) Prost, L. R., Daley, M. E., Le Sage, V., Bader, M. W., Le Moual, H., Klevit, R. E., and Miller, S. I. (2007) Activation of the bacterial sensor kinase phoQ by acidic pH. *Mol. Cell* 26, 165–174.

(45) Kwak, S.-Y., Wiedemann-Bidlack, R. B., Beniash, E., Yamakoshi, Y., Simmer, J. P., Litman, A., and Margolis, H. C. (2009) Role of 20-kDa amelogenin (P148) phosphorylation in calcium phosphate formation in vitro. *J. Biol. Chem.* 284, 18972–18979.

(46) Brookes, S., Kirkham, J., Shore, R., Bonass, W., and Robinson, C. (1998) Enzyme compartmentalization during biphasic enamel matrix processing. *Connect. Tissue Res.* 3, 89–99.